

# Likely chirality of stochastic anisotropic hyperelastic tubes

L. Angela Mihai\*    Thomas E. Woolley†    Alain Goriely‡

January 27, 2023

## Abstract

When an elastic tube reinforced with helical fibres is inflated, its ends rotate. In large deformations, the amount and chirality of rotation is highly non-trivial as it depends on the choice of strain-energy density and the arrangements of the fibres. In the case where the material parameters are fixed, the problem has been satisfactorily addressed. However, in many systems, the material parameters are not precisely known, and it is therefore more appropriate to treat them as random variables. The problem is then to understand chirality in a stochastic framework. Here, we examine the elastic responses of a stochastic anisotropic hyperelastic tube, where the material parameters are generated from known probability density functions, subjected to uniform dead loading consisting of internal pressure, axial tension and torque. Assuming that the tube wall is thin and that the resulting deformation is the combined inflation, extension and torsion from the reference circular cylindrical configuration to a deformed circular cylindrical state, we derive the probabilities of radial expansion or contraction, and of right-handed or left-handed torsion. We refer to these stochastic behaviours as ‘likely inflation’ and ‘likely chirality’ respectively.

**Key words:** stochastic elasticity; anisotropic material; chirality; applied probability.

## 1 Introduction

Biological, medical, and engineering applications of the extension-torsion-inflation couplings in pressurised circular tubes with helical anisotropy range from plant and animal tissues [4, 20] to cardiac and vascular systems [9, 37] to soft actuators [5, 6] and dielectric elastomers [14]. The mechanical effects of the stiffness and orientation of the fibres winding helically around the tube’s axis were analysed in detail, within the framework of finite elasticity, in [11]. There it was shown that: (i) the tube can lengthen or increase in girth depending on the fibre orientation and the relative stiffness of the matrix and fibres; (ii) when the fibres are equal in stiffness and orientation, the tube may exhibit no rotation; (iii) a tube with a single pre-compressed right-handed fibre may rotate either clockwise or anti-clockwise depending on the material parameters, showing that transfer of chirality under external loads from the tube-wall micro-structure to the tubular macro-structure relies both on geometry and material properties.

In addition, for many solid materials, a crucial part in assessing their physical properties is to quantify the uncertainties in their mechanical responses, which cannot be ignored [15, 34, 36]. In finite elasticity, the use of the information about uncertainties [47] and the variability in the observational data has recently been proposed by the introduction of stochastic hyperelastic models, characterised by a stochastic strain-energy function, where the model parameters are random variables that satisfy standard probability laws [28, 43–46]. These are phenomenological models that are based on the notion of entropy (or uncertainty) [38] and the maximum entropy principle for a discrete probability distribution [16–18], and are able to propagate uncertainties from input data to output quantities

---

\*School of Mathematics, Cardiff University, Senghennydd Road, Cardiff, CF24 4AG, UK, Email: MihaiLA@cardiff.ac.uk

†School of Mathematics, Cardiff University, Senghennydd Road, Cardiff, CF24 4AG, UK, Email: WoolleyT1@cardiff.ac.uk

‡Mathematical Institute, University of Oxford, Woodstock Road, Oxford, OX2 6GG, UK, Email: goriely@maths.ox.ac.uk

of interest. For these models, the mathematical question arises: *what is the influence of probabilistic model parameters on the predicted elastic responses?* This question has begun to be addressed in [29–31], with the tractable special cases of stochastic hyperelastic bodies with simple geometries for which the finite deformation is prescribed. Specifically, the sensitive dependence on parameter probabilities of the stability under critical dead loads was demonstrated by showing that, in contrast to the deterministic elastic problem, where a single critical value strictly separates the cases where instability can or cannot occur, for the stochastic problem, there is a probabilistic interval where the two cases always compete in the sense that both have a quantifiable chance to be found. More complex, but still tractable problems, can be treated in a similar manner.

In this paper, we examine the elastic responses under dead loading of a hyperelastic cylindrical tube of stochastic anisotropic material. The dead loading consists of simultaneous internal pressure, axial tension and torque, and the resulting universal deformation is a combined inflation, extension and torsion from the reference circular cylindrical configuration to a deformed, also circular cylindrical, state. For the anisotropic material, two non-orthogonal preferred directions are assumed, corresponding to the (mean) directions of two families of aligned fibres embedded in an isotropic matrix material. In the deterministic elastic case, the tube may undergo ‘inversion’ in the deformation, such that the radius first decreases and then increases, or ‘perversion’ whereby the torsion chirality changes from right-handed to left-handed [12, 23]. The possible existence of such responses depends on the material constitutive model. For the stochastic problem, we derive the probability distribution of the deformations, and find that, due to the probabilistic nature of the material parameters, the different states always compete. In particular, at a critical load, the radius may decrease or increase with a given probability, and we refer to this phenomenon as ‘likely inflation’, and similarly, right-handed or left-handed torsion may occur with a given probability, and we refer to this as ‘likely chirality’. In Section 2, the kinematics of finite simple torsion superposed on uniform stretch for circular cylindrical tubes is briefly reviewed. In Section 3, the stochastic elastic modelling framework is presented. In Section 4, the probabilistic solution for the stochastic tubes is obtained. Concluding remarks are provided in Section 5.

## 2 Stretch and torsion of a circular cylindrical tube

We consider a circular cylindrical tube occupying the reference domain  $(R, \Theta, Z) \in [A, B] \times [-\pi, \pi) \times [0, H]$ , where  $A$ ,  $B$  and  $H$  are positive constants, subject to the combined deformation consisting of simple torsion superposed on on axial stretch [48, pp. 184–186],

$$r = \sqrt{a^2 + \frac{R^2 - A^2}{\xi}}, \quad \theta = \Theta + \tau\zeta Z, \quad z = \zeta Z, \quad (1)$$

where  $(r, \theta, z) \in [a, b] \times [-\pi, \pi) \times [0, h]$  are the cylindrical polar coordinates in the deformed configuration,  $a$ ,  $\tau$  and  $\zeta$  are given positive constants,  $b = \sqrt{a^2 + (B^2 - A^2)/\zeta}$ , and  $h = \zeta H$  (see Figure 1).

Through the deformation (1), the circular plane section at  $Z = 0$  remains fixed and each circular plane section normal to the central axis remains plane and rotates by an angle  $\tau\zeta Z$ . Denoting

$$\lambda = \frac{r}{R} = \frac{1}{R} \sqrt{a^2 + \frac{R^2 - A^2}{\zeta}}, \quad (2)$$

the deformation gradient in terms of the current cylindrical polar coordinates  $(r, \theta, z)$  is equal to

$$\mathbf{F} = \begin{bmatrix} \partial r / \partial R & 0 & 0 \\ 0 & (r/R) \partial \theta / \partial \Theta & r \partial \theta / \partial Z \\ 0 & 0 & \partial z / \partial Z \end{bmatrix} = \begin{bmatrix} 1/(\lambda\zeta) & 0 & 0 \\ 0 & \lambda & \tau\zeta r \\ 0 & 0 & \zeta \end{bmatrix}, \quad (3)$$

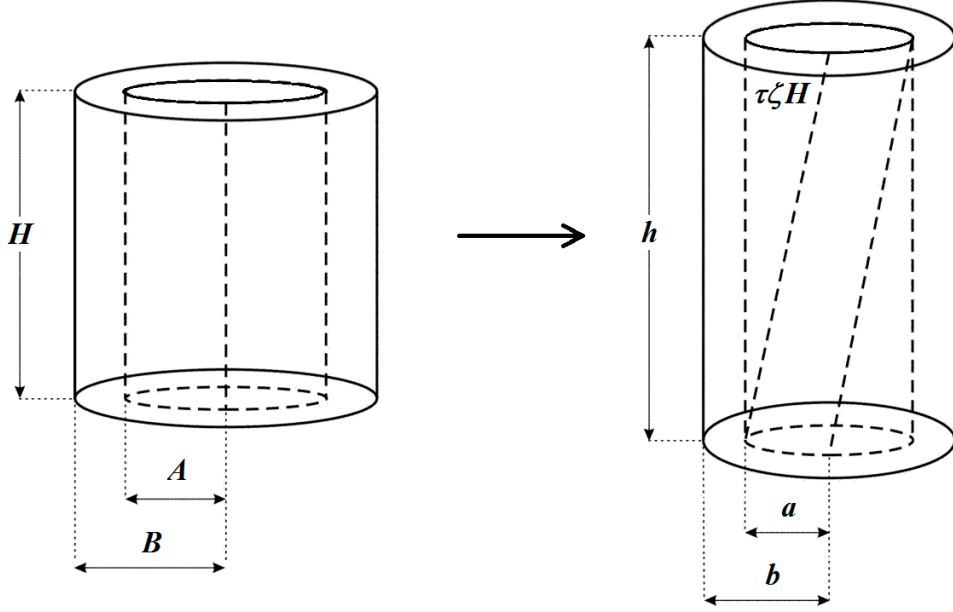


Figure 1: Schematic of circular cylindrical tube (left) deformed by combined stretch and torsion (right).

and the left and right Cauchy-Green tensors are, respectively,

$$\mathbf{B} = \mathbf{F}\mathbf{F}^T = \begin{bmatrix} 1/(\lambda^2\zeta^2) & 0 & 0 \\ 0 & \lambda^2 + \tau^2\zeta^2r^2 & \tau\zeta^2r \\ 0 & \tau\zeta^2r & \zeta^2 \end{bmatrix}, \quad (4)$$

$$\mathbf{C} = \mathbf{F}^T\mathbf{F} = \begin{bmatrix} 1/(\lambda^2\zeta^2) & 0 & 0 \\ 0 & \lambda^2 & \tau\zeta r\lambda \\ 0 & \tau\zeta r\lambda & \zeta^2(\tau^2r^2 + 1) \end{bmatrix}. \quad (5)$$

Then, if we denote  $\lambda_a = a/A$ , by (2), we obtain

$$\lambda_b = \frac{b}{B} = \frac{1}{B} \sqrt{a^2 + \frac{B^2 - A^2}{\zeta}} \quad (6)$$

and

$$r = A\lambda\sqrt{1 - \lambda_a^2\zeta}(1 - \lambda^2\zeta). \quad (7)$$

Next, assuming that the components of the Cauchy stress,  $\mathbf{T}$ , are independent of  $\theta$  and  $z$ , the equilibrium equations are reduced to [48, p. 185],

$$\begin{aligned} \frac{\partial T_{rr}}{\partial r} + \frac{T_{rr} - T_{\theta\theta}}{r} &= 0, \\ \frac{\partial T_{r\theta}}{\partial r} + 2\frac{T_{r\theta}}{r} &= 0, \\ \frac{\partial T_{rz}}{\partial r} + \frac{T_{rz}}{r} &= 0, \end{aligned} \quad (8)$$

and, by further assuming that  $T_{r\theta} = 0$  and  $T_{rz} = 0$ , it follows that

$$\frac{dT_{rr}}{dr} = \frac{T_{\theta\theta} - T_{rr}}{r}. \quad (9)$$

Hence,

$$T_{\theta\theta} = \frac{d(rT_{rr})}{dr}. \quad (10)$$

In this case, by applying a uniform internal pressure, the outer surface of the cylinder may be rendered free of traction, such that  $T_{rr} = 0$  on  $r = B$ . Then, for an internally pressurised tube which is free on the outer surface, we have

$$T_{rr}|_{r=a} = -P, \quad T_{rr}|_{r=b} = 0, \quad (11)$$

where  $P > 0$  is constant. Integrating the first equation in (9) with respect to  $r$  and substituting in the first condition given in (11), we obtain

$$P = \int_a^b \frac{T_{\theta\theta} - T_{rr}}{r} dr. \quad (12)$$

For the deformation (1), by (10), the resultant normal force acting upon the plane  $a \leq r \leq b$ ,  $z$ -constant,  $|\theta| \leq \pi$  is calculated as follows [48, pp. 185],

$$\begin{aligned} N &= 2\pi \int_a^b T_{zz} r dr, \\ &= 2\pi \int_a^b (T_{zz} - T_{rr}) r dr + 2\pi \int_a^b T_{rr} r dr, \\ &= 2\pi \int_a^b (T_{zz} - T_{rr}) r dr + \pi \int_a^b T_{rr} r^2 dr + \pi \int_a^b (T_{rr} - T_{\theta\theta}) r dr, \\ &= \pi P a^2 + \pi \int_a^b (2T_{zz} - T_{rr} - T_{\theta\theta}) r dr. \end{aligned} \quad (13)$$

Equivalently,

$$N = \pi P a^2 + F, \quad (14)$$

where

$$F = \pi \int_a^b (2T_{zz} - T_{rr} - T_{\theta\theta}) r dr. \quad (15)$$

The resulting twisting moment is equal to [48, p. 190],

$$T = 2\pi \int_a^b T_{\theta z} r^2 dr. \quad (16)$$

By applying the change of variable (7), the expressions of  $P$ ,  $F$ , and  $T$ , given by (12), (15), and (16) respectively, take the following equivalent forms,

$$P = \int_{\lambda_a}^{\lambda_b} \frac{T_{\theta\theta} - T_{rr}}{\lambda(1 - \lambda^2\zeta)} d\lambda, \quad (17)$$

$$F = \pi A^2 \int_{\lambda_a}^{\lambda_b} \lambda (2T_{zz} - T_{rr} - T_{\theta\theta}) \frac{1 - \lambda_a^2\zeta}{(1 - \lambda^2\zeta)^2} d\lambda, \quad (18)$$

$$T = 2\pi A^3 \int_{\lambda_a}^{\lambda_b} \lambda^2 T_{\theta z} \frac{(1 - \lambda_a^2\zeta)^{3/2}}{(1 - \lambda^2\zeta)^{5/2}} d\lambda. \quad (19)$$

### 3 Stochastic anisotropic hyperelastic material

In this Section, we combine finite elasticity [10, 35, 48] and probability theory [13, 18], and consider a tube made of a stochastic homogeneous hyperelastic material for which the given parameters are *random variables* that satisfy standard probability laws [28, 43–45]. For each model parameter, the partial information provided by the *mean value* and *variance* is commonly used [7, 15, 22, 33]. Specifically, we assume that the tube is made of an aeolotropic material with two preferred directions with respect to the reference configuration induced by two families of aligned extensible fibres embedded in an isotropic matrix material. The two preferred direction are taken, respectively, [11], [10, pp. 328–336]

$$\mathbf{M}_1 = \begin{bmatrix} M_{1r} \\ M_{1\theta} \\ M_{1z} \end{bmatrix} = \begin{bmatrix} 0 \\ \cos \Phi \\ \sin \Phi \end{bmatrix} \quad \text{and} \quad \mathbf{M}_2 = \begin{bmatrix} M_{2r} \\ M_{2\theta} \\ M_{2z} \end{bmatrix} = \begin{bmatrix} 0 \\ -\cos \Psi \\ \sin \Psi \end{bmatrix} \quad (20)$$

where  $\Phi, \Psi \in [0, \pi/2]$ . Then, under the deformation (1), the stretch ratios of the fibres,  $\lambda_4$  and  $\lambda_6$  respectively, are given by

$$I_4 = \lambda_4^2 = (\mathbf{C}\mathbf{M}_1) \cdot \mathbf{M}_1, \quad I_6 = \lambda_6^2 = (\mathbf{C}\mathbf{M}_2) \cdot \mathbf{M}_2, \quad (21)$$

where  $\mathbf{C}$  is the right Cauchy-Green tensor defined by (5).

For such a material, the strain-energy function depends on seven independent invariants [2, 3], including the principal invariants,  $I_1, I_2, I_3$ , of the Cauchy-Green tensors  $\mathbf{B}$  and  $\mathbf{C}$  [42],  $I_4$  and  $I_6$  given by (21), and two other invariants defined as follows,

$$I_5 = (\mathbf{C}^2\mathbf{M}_1) \cdot \mathbf{M}_1, \quad I_7 = (\mathbf{C}^2\mathbf{M}_2) \cdot \mathbf{M}_2. \quad (22)$$

Here, we restrict our attention to the simplest case of an incompressible stochastic anisotropic hyperelastic model containing two families of extensible fibres embedded in a neo-Hookean material, and characterised by the following strain-energy function,

$$\mathcal{W}(I_1, I_4, I_6) = \frac{\mu_1}{2} (I_1 - 3) + \frac{\mu_4}{4} (I_4 - 1)^2 + \frac{\mu_6}{4} (I_6 - 1)^2, \quad (23)$$

where  $\mu, \mu_4$  and  $\mu_6$  are positive random-field parameters drawn from known probability distributions. In the deterministic elastic case,  $\mu, \mu_4$  and  $\mu_6$  are constants, and  $\mu > 0$  represents the shear modulus for the infinitesimal deformation [27].

For the stochastic material described by (23), the following mathematical constraints [28–31, 43–45],

$$\begin{cases} E[\mu] = \underline{\mu} > 0, \\ E[\log \mu] = \nu, \quad \text{such that } |\nu| < +\infty, \end{cases} \quad (24)$$

guarantee the random shear modulus,  $\mu$ , and its inverse,  $1/\mu$ , are second-order random variables, i.e., they have finite mean value and finite variance [40, 41]. Then, the random shear modulus,  $\mu > 0$ , with mean value  $\underline{\mu}$  and variance  $\text{Var}[\mu]$ , follows a Gamma probability distribution [40, 41], with shape parameter  $\rho_1 > 0$  and scale parameter  $\rho_2 > 0$  defined by

$$\rho_1 = \frac{\underline{\mu}^2}{\text{Var}[\mu]}, \quad \rho_2 = \frac{\text{Var}[\mu]}{\underline{\mu}}. \quad (25)$$

The corresponding probability density function takes the form [1, 19]

$$g(\mu; \rho_1, \rho_2) = \frac{\mu^{\rho_1-1} e^{-\mu/\rho_2}}{\rho_2^{\rho_1} \Gamma(\rho_1)}, \quad \text{for } \mu > 0 \text{ and } \rho_1, \rho_2 > 0, \quad (26)$$

where  $\Gamma : \mathbb{R}_+^* \rightarrow \mathbb{R}$  is the complete Gamma function

$$\Gamma(z) = \int_0^{+\infty} t^{z-1} e^{-t} dt. \quad (27)$$

Similarly, by setting the mathematical expectations [46]

$$\begin{cases} E[\mu_4] = \underline{\mu}_4 > 0, \\ E[\log \mu_4] = \nu_4, \quad \text{such that } |\nu_4| < +\infty, \end{cases} \quad (28)$$

and

$$\begin{cases} E[\mu_6] = \underline{\mu}_6 > 0, \\ E[\log \mu_6] = \nu_6, \quad \text{such that } |\nu_6| < +\infty, \end{cases} \quad (29)$$

the random parameters  $\mu_4 > 0$  and  $\mu_6 > 0$ , with mean values  $\underline{\mu}_4$  and  $\underline{\mu}_6$ , and variance  $\text{Var}[\mu_4]$  and  $\text{Var}[\mu_6]$  respectively, follow the Gamma probability distributions with shape and scale parameters defined, respectively, by

$$\rho_1^{(4)} = \frac{\underline{\mu}_4^2}{\text{Var}[\mu_4]}, \quad \rho_2^{(4)} = \frac{\text{Var}[\mu_4]}{\underline{\mu}_4}, \quad (30)$$

and

$$\rho_1^{(6)} = \frac{\underline{\mu}_6^2}{\text{Var}[\mu_6]}, \quad \rho_2^{(6)} = \frac{\text{Var}[\mu_6]}{\underline{\mu}_6}, \quad (31)$$

and we denote by  $g_4(u; \rho_1^{(4)}, \rho_2^{(4)})$  and  $g_6(u; \rho_1^{(4)}, \rho_2^{(4)})$  the corresponding probability distributions.

## 4 Inflation and torsion of a stochastic anisotropic tube

For a cylindrical tube of stochastic anisotropic hyperelastic material with the strain-energy density function  $\mathcal{W}$  given by (23), subject to the deformation (1), the Cauchy stress tensor takes the form

$$\mathbf{T} = -p\mathbf{I} + \beta_1\mathbf{B} + \beta_4\mathbf{F}\mathbf{M}_1 \otimes \mathbf{F}\mathbf{M}_1 + \beta_6\mathbf{F}\mathbf{M}_2 \otimes \mathbf{F}\mathbf{M}_2, \quad (32)$$

where  $\mathbf{B}$  is the left Cauchy-Green tensor described by (4),  $\beta_i = 2\partial\mathcal{W}/\partial I_i$ ,  $i = 1, 4, 6$ , are the material response coefficients, and  $p$  is the Lagrange multiplier for the incompressibility constraint,  $\det \mathbf{F} = 1$ . The preferred directions given by (20) are deformed into the following directions respectively,

$$\mathbf{m}_1 = \mathbf{F}\mathbf{M}_1 = \begin{bmatrix} 0 \\ \lambda \cos \Phi + \tau \zeta r \sin \Phi \\ \zeta \sin \Phi \end{bmatrix}, \quad \mathbf{m}_2 = \mathbf{F}\mathbf{M}_2 = \begin{bmatrix} 0 \\ -\lambda \cos \Psi + \tau \zeta r \sin \Psi \\ \zeta \sin \Psi \end{bmatrix}. \quad (33)$$

Thus, the non-zero components of the stress tensor given by (32) take the form,

$$\begin{aligned} T_{rr} &= -p + \frac{\beta_1}{\lambda^2 \zeta^2}, \\ T_{\theta\theta} &= -p + \beta_1 (\lambda^2 + \tau^2 \zeta^2 r^2) + \beta_4 (\lambda \cos \Phi + \tau \zeta r \sin \Phi)^2 + \beta_6 (\lambda \cos \Psi - \tau \zeta r \sin \Psi)^2, \\ T_{\theta z} &= \beta_1 \tau \zeta^2 r + \beta_4 \zeta \sin \Phi (\lambda \cos \Phi + \tau \zeta r \sin \Phi) - \beta_6 \zeta \sin \Psi (\lambda \cos \Psi - \tau \zeta r \sin \Psi), \\ T_{zz} &= -p + \beta_1 \zeta^2 + \beta_4 \zeta^2 \sin^2 \Phi + \beta_6 \zeta^2 \sin^2 \Psi. \end{aligned} \quad (34)$$

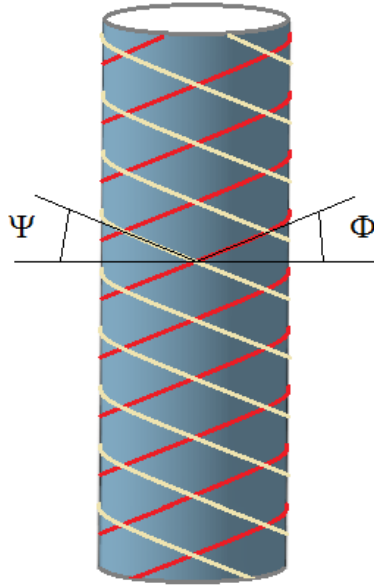


Figure 2: Schematic of anisotropic cylindrical shell of anisotropic material, showing the orientation of the preferred directions induced by two families of aligned fibres tangential to the cylindrical surface.

Assuming that the tube wall is thin (see Figure 2), we set  $A = 1$  and  $B = 1 + \epsilon$ , and represent  $P$ ,  $F$ , and  $T$ , given by (17), (18), and (19) respectively, as the following series expansions [11]

$$P = P^{(0)} + P^{(1)}\epsilon + P^{(2)}\epsilon^2 + \dots, \quad (35)$$

$$F = F^{(0)} + F^{(1)}\epsilon + F^{(2)}\epsilon^2 + \dots, \quad (36)$$

$$T = T^{(0)} + T^{(1)}\epsilon + T^{(2)}\epsilon^2 + \dots, \quad (37)$$

where we assume that  $P^{(0)} = F^{(0)} = T^{(0)} = 0$ . We then truncate the series given by (35), (36), and (37) respectively, to first order in  $\epsilon$ , as follows,

$$P = \frac{1}{\zeta} \left[ \mu \left( \zeta^2 \tau^2 + 1 - \frac{1}{\lambda^4 \zeta^2} \right) + \mu_4 J_4 (\cos \Phi + \tau \zeta \sin \Phi)^2 + \mu_6 J_6 (\cos \Psi - \tau \zeta \sin \Psi)^2 \right], \quad (38)$$

$$F = -\frac{\pi}{\zeta} \left[ \mu \left( \lambda^2 \zeta^2 \tau^2 - 2\zeta^2 + \lambda^2 + \frac{1}{\lambda^2 \zeta^2} \right) + \mu_4 J_4 (J_4 + 1 - 3\zeta \sin^2 \Phi) + \mu_6 J_6 (J_6 + 1 - 3\zeta \sin^2 \Psi) \right], \quad (39)$$

$$T = 2\pi\lambda [\mu\lambda\zeta\tau + \mu_4 J_4 \lambda \sin \Phi (\cos \Phi + \zeta\tau \sin \Phi) + \mu_6 J_6 \lambda \sin \Psi (\cos \Psi - \zeta\tau \sin \Psi)], \quad (40)$$

where

$$J_4 = I_4 - 1 = \lambda^2 \cos^2 \Phi + 2\lambda^2 \zeta \tau \cos \Phi \sin \Phi + \zeta^2 \sin^2 \Phi (\lambda^2 \tau^2 + 1) - 1, \quad (41)$$

$$J_6 = I_6 - 1 = \lambda^2 \cos^2 \Psi - 2\lambda^2 \zeta \tau \cos \Psi \sin \Psi + \zeta^2 \sin^2 \Psi (\lambda^2 \tau^2 + 1) - 1. \quad (42)$$

Next, we define the following Jacobian matrix [11]

$$\mathbf{J} = (J_{ij})_{i,j=1,2,3} = \begin{bmatrix} \partial P / \partial \lambda & \partial P / \partial \zeta & \partial P / \partial \tau \\ \partial F / \partial \lambda & \partial F / \partial \zeta & \partial F / \partial \tau \\ \partial T / \partial \lambda & \partial T / \partial \zeta & \partial T / \partial \tau \end{bmatrix}, \quad (43)$$

and concentrate our attention on infinitesimal deformations close to the reference configuration  $(\lambda, \zeta, \tau) = (1, 1, 0)$ , where  $\mathbf{J}|_{(1,1,0)}$  has the following components,

$$\begin{aligned} J_{11}|_{(1,1,0)} &= \frac{\partial P}{\partial \lambda}|_{(1,1,0)} = 4\mu + 2\mu_4 \cos^4 \Phi + 2\mu_6 \cos^4 \Psi, \\ J_{12}|_{(1,1,0)} &= \frac{\partial P}{\partial \zeta}|_{(1,1,0)} = 2\mu + 2\mu_4 \cos^2 \Phi \sin^2 \Phi + 2\mu_6 \cos^2 \Psi \sin^2 \Psi, \\ J_{13}|_{(1,1,0)} &= \frac{\partial P}{\partial \tau}|_{(1,1,0)} = 2\mu_4 \cos^3 \Phi \sin \Phi - 2\mu_6 \cos^3 \Psi \sin \Psi, \\ J_{21}|_{(1,1,0)} &= \frac{\partial F}{\partial \lambda}|_{(1,1,0)} = 2\pi\mu_4 \cos^2 \Phi (3 \sin^2 \Phi - 1) + 2\pi\mu_6 \cos^2 \Psi (3 \sin^2 \Psi - 1), \\ J_{22}|_{(1,1,0)} &= \frac{\partial F}{\partial \zeta}|_{(1,1,0)} = 6\pi\mu + 2\pi\mu_4 \sin^2 \Phi (3 \sin^2 \Phi - 1) + 2\pi\mu_6 \sin^2 \Psi (3 \sin^2 \Psi - 1), \\ J_{23}|_{(1,1,0)} &= \frac{\partial F}{\partial \tau}|_{(1,1,0)} = 2\pi\mu_4 \cos \Phi \sin \Phi (3 \sin^2 \Phi - 1) - 2\pi\mu_6 \cos \Psi \sin \Psi (3 \sin^2 \Psi - 1), \\ J_{31}|_{(1,1,0)} &= \frac{\partial T}{\partial \lambda}|_{(1,1,0)} = 4\pi\mu_4 \cos^3 \Phi \sin \Phi - 4\pi\mu_6 \cos^3 \Psi \sin \Psi, \\ J_{32}|_{(1,1,0)} &= \frac{\partial T}{\partial \zeta}|_{(1,1,0)} = 4\pi\mu_4 \cos \Phi \sin^3 \Phi - 4\pi\mu_6 \cos \Psi \sin^3 \Psi, \\ J_{33}|_{(1,1,0)} &= \frac{\partial T}{\partial \tau}|_{(1,1,0)} = 2\pi\mu + 4\pi\mu_4 \cos^2 \Phi \sin^2 \Phi + 4\pi\mu_6 \cos^2 \Psi \sin^2 \Psi. \end{aligned} \quad (44)$$

Assuming that  $\det \mathbf{J}|_{(1,1,0)} \neq 0$ , we can define the matrix inverse

$$\mathbf{A} = (A_{ij})_{i,j=1,2,3} = \mathbf{J}^{-1}|_{(1,1,0)}. \quad (45)$$

This will be useful when exploring the critical points where an inversion in the deformation occurs.

In order to obtain clear explicit results, in the subsequent analysis, we limit our investigation to the case where the two families of fibres have the same material properties, i.e.,  $\mu_4 = \mu_6$ , and recall that  $\mu$  follows a Gamma probability distribution  $g(u; \rho_1, \rho_2)$ , defined by (26), and  $\mu_4$  follows a Gamma distribution,  $g_4(u; \rho_1^{(4)}, \rho_2^{(4)})$ . We further assume that  $\mu$  and  $\mu_4$  are stochastically independent random variables [46]. Then, the probability distribution for the random shear moduli of the material under infinitesimal deformations in different directions can be computed by employing the usual summation formulae [21, 32], and for real materials, these assumptions can be verified through suitable experimental tests, at least in principle. This is an important aspect regarding the constitutive behaviour of anisotropic stochastic hyperelastic materials, which deserves further investigation. However, to illustrate our theoretical results, numerical examples of the Gamma distributions considered here are represented in Figure 3, where the shape and scale parameters are  $\rho_1 = 405$  and  $\rho_2 = 0.01$  for the random shear modulus  $\mu > 0$ , and  $\rho_1^{(4)} = \rho_1 = 405$  and  $\rho_2^{(4)} = 20\rho_2 = 0.2$ , for the random parameter  $\mu_4 = 20\mu > 0$ . Note that, although Gamma distributions are used throughout this paper, the distributions in Figure 3 appear to be approximately normal distributions. This is not a coincidence and we have illustrated in a previous paper [29] that such a comparison is favourable whenever  $\rho_1$  is large when compared to  $\rho_2$ .

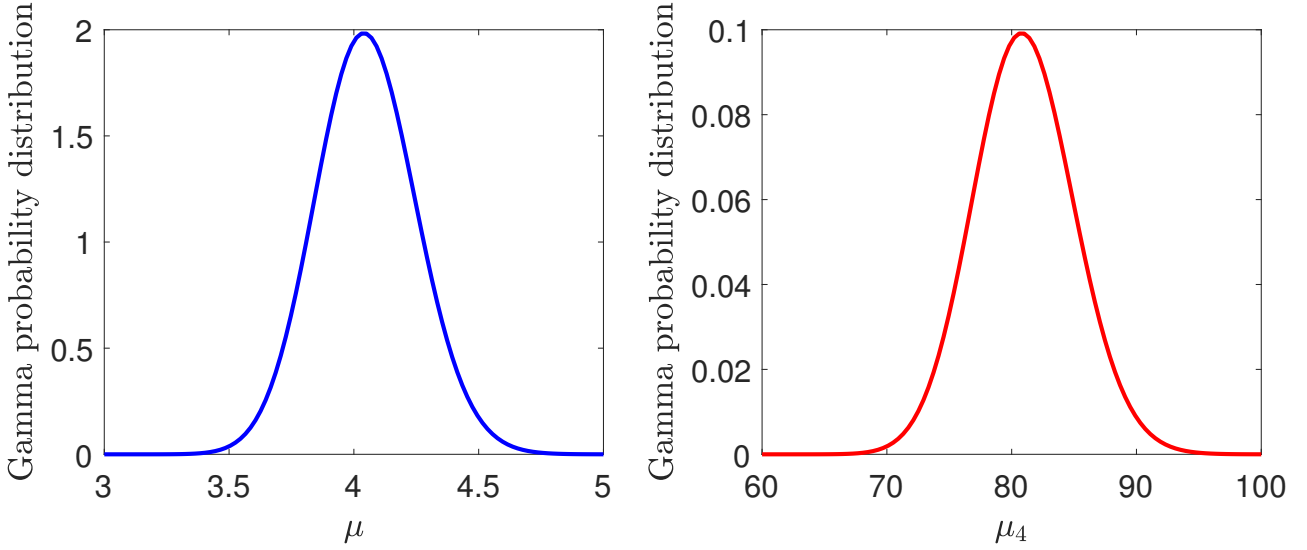


Figure 3: Examples of Gamma distribution with  $\rho_1 = 405$  and  $\rho_2 = 0.01$  for  $\mu > 0$  (left), and  $\rho_1^{(4)} = 405$  and  $\rho_2^{(4)} = 0.2$ , for  $\mu_4 > 0$  (right).

#### 4.1 Likely inflation of the stochastic tube

First, we assume that  $\Phi = \Psi$  [11], and consider the critical point for radial stretch  $\lambda$ , such that

$$A_{11} = 0, \quad \text{where} \quad A_{11} = \frac{\mu_4 [3 \cos^2(2\phi) - 4 \cos(2\phi) + 1] + 6\mu}{8\mu [3\mu_4 \cos^2(2\phi) + \mu_4 + 3\mu]}. \quad (46)$$

The radial stretch increases if  $A_{11} > 0$  and decreases if  $A_{11} < 0$ , and equation (46) is equivalent to the following quadratic equation in  $\cos(2\Phi)$ ,

$$\mu_4 [3 \cos^2(2\Phi) - 4 \cos(2\Phi) + 1] + 6\mu = 0, \quad (47)$$

which has real solutions when  $0 < \mu \leq \mu_4/18$ . As the denominator of  $A_{11}$  is positive, it follows that, as the internal pressure increases, the radial stretch  $\lambda$  increases if  $\mu > \mu_4/18$  and decreases if  $0 < \mu < \mu_4/18$ .

In this case, the probability distribution of stable inflation, such that the radial stretch monotonically increases when the internal pressure increases, is

$$P_1(\mu_4) = 1 - \int_0^{\mu_4/18} g(u; \rho_1, \rho_2) du, \quad (48)$$

and that of unstable inflation, whereby the radial stretch starts to decrease under increasing pressure, is

$$P_2(\mu_4) = 1 - P_1(\mu_4). \quad (49)$$

Taking  $\rho_1 = 405$  and  $\rho_2 = 0.01$  (see Figure 3 - left), the mean value of the shear modulus is  $\underline{\mu} = \rho_1 \rho_2 = 4.05$ , and the probability distributions given by equations (48)-(49) are illustrated in Figure 4 (blue lines for  $P_1$  and red lines for  $P_2$ ). Specifically,  $\mu_4 \in (0, 36\underline{\mu})$  was divided into 100 steps, then for each value of  $\mu_4$ , 100 random values of  $\mu$  were numerically generated from the specified Gamma distribution and compared with the inequalities defining the two intervals for values of  $\mu_4$ . For the deterministic elastic case, which is based on the mean value of the shear modulus,  $\underline{\mu} = \rho_1 \rho_2 = 4.05$ , the critical value of  $\mu_4 = 18\underline{\mu} = 72.9$  strictly separates the cases where radial stretch instability can, and cannot, occur. For the stochastic problem, for the same critical value, there is, by definition, exactly 50% chance that radial stretch is stable (blue lines) and 50% chance that instability occurs (red lines). To increase the probability of stable radial stretch ( $P_1 \approx 1$ ), one must consider values of  $\mu_4$  that are sufficiently smaller than the expected critical value, whereas an instability is certain



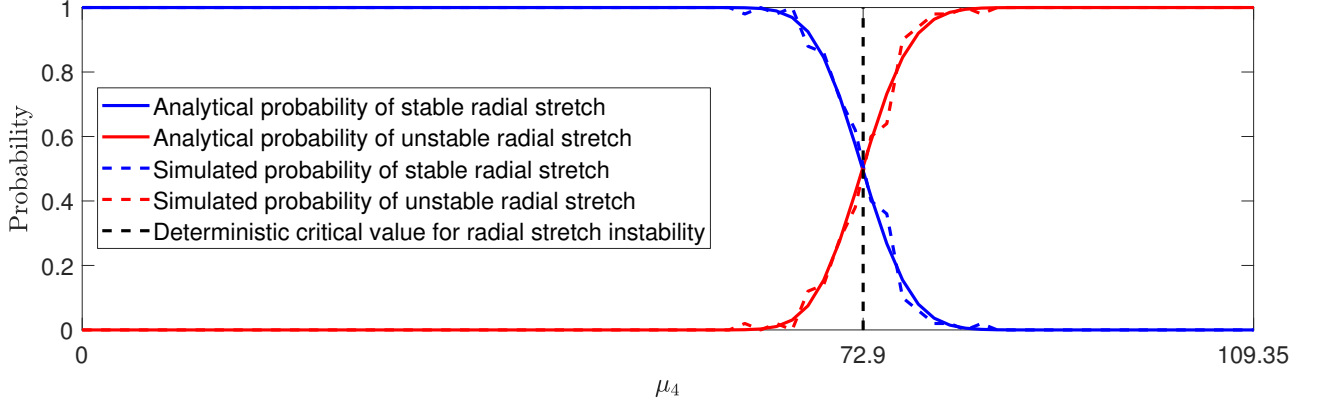


Figure 4: Probability distributions of whether radial stretch instability can occur or not for an anisotropic cylindrical tube of stochastic hyperelastic material described by (23) with the shear modulus,  $\mu$ , following a Gamma distribution with  $\rho_1 = 405$ ,  $\rho_2 = 0.01$ , and  $\mu_4$  following a Gamma distribution with  $\rho_1^{(4)} = 405$ ,  $\rho_2^{(4)} = 0.2$ . Continuous coloured lines represent analytically derived solutions, given by equations (48)-(49), whereas the dashed versions represent stochastically generated data. The vertical line at the critical value,  $\mu_4 = 72.9$ , separates the expected regions based only on the mean value of the shear modulus,  $\underline{\mu} = \rho_1 \rho_2 = 4.05$ . The probabilities were calculated from the average of 50 stochastic simulations.

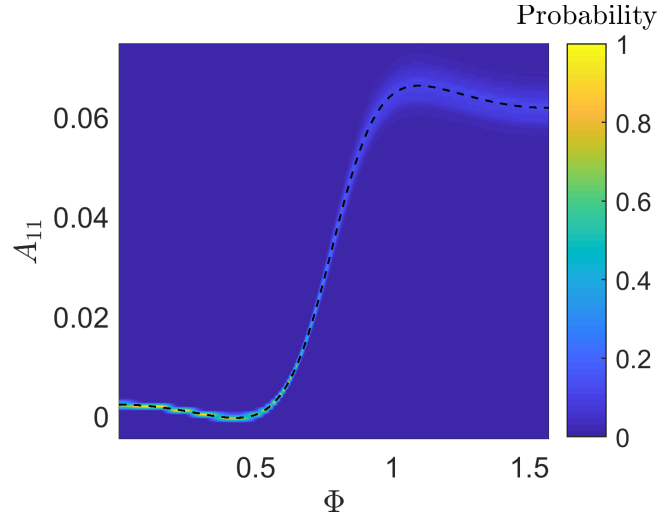


Figure 5: Probability distribution of stochastic  $A_{11}$ , for the inflation of an anisotropic cylindrical tube of stochastic hyperelastic material, given by (23) with the shear modulus,  $\mu$ , drawn from a Gamma distribution with  $\rho_1 = 405$ ,  $\rho_2 = 0.01$ , and  $\mu_4$  drawn from a Gamma distribution with  $\rho_1^{(4)} = 405$ ,  $\rho_2^{(4)} = 0.2$ . As  $\underline{\mu} = \rho_1 \rho_2 = 4.05 < \underline{\mu}_4/18 = \rho_1^{(4)} \rho_2^{(4)}/18 = 4.5$ , instability is expected to occur, but there is also around 2% chance that the radial stretch is stable. The dashed black line corresponds to the expected value of  $A_{11}$  based only on mean parameter values. Each distribution was calculated from the average of  $10^3$  stochastic simulations.

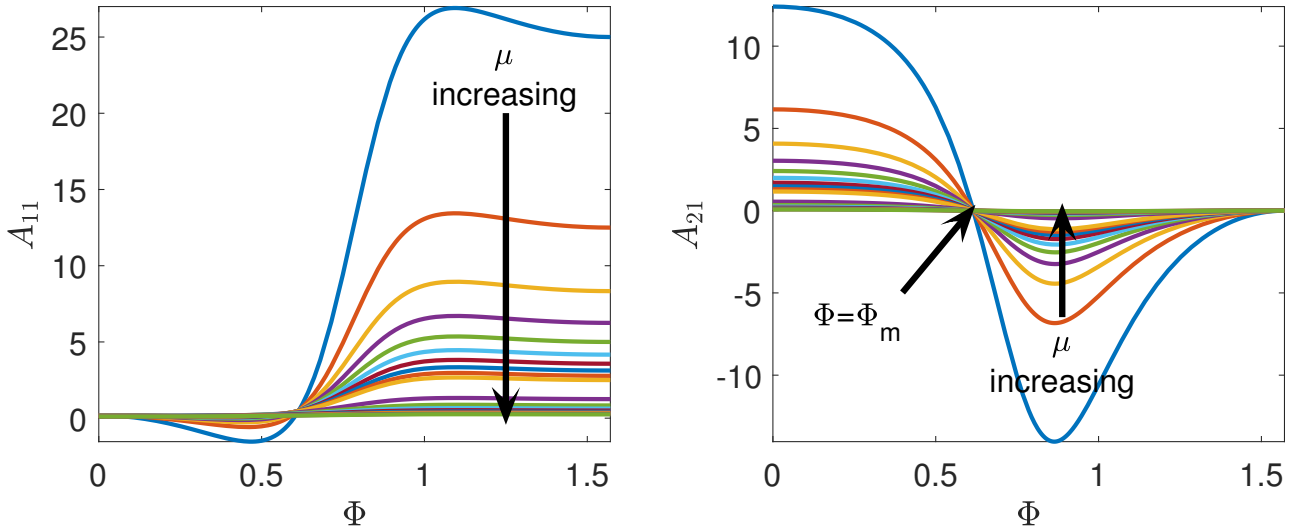


Figure 6: Deterministic values of  $A_{11}$  (left) and  $A_{21}$  (right), for  $\mu_4 = 1$  and  $\mu \in \{0.01, 0.02, \dots, 0.1, 0.2, \dots, 1\}$  (the direction of increasing values of  $\mu$  is indicated by arrow).

to occur ( $P_2 \approx 1$ ) for values of  $\mu_4$  which are sufficiently greater than the expected critical value. However, the inherent variability in the probabilistic system means that there exist events where there is competition between the two cases.

To illustrate this, in Figure 5, we represent the probability distribution of  $A_{11}$  as a function of the angle  $\Phi$  when  $\mu$  follows a Gamma distribution with  $\rho_1 = 405$ ,  $\rho_2 = 0.01$ , and  $\mu_4$  follows a Gamma distribution with  $\rho_1^{(4)} = 405$ ,  $\rho_2^{(4)} = 0.2$ , as shown in Figure 3. In this case,  $\underline{\mu}_4 = 20\mu < 81$ , and unstable radial stretch is expected. Nevertheless, the probability distribution suggests that there is also around 2% chance that the radial stretch is stable.

For the axial stretch  $\zeta$ , the critical value satisfies the equation

$$A_{21} = 0 \quad \text{where} \quad A_{21} = \frac{\mu_4 [3 \cos^2(2\phi) + 2 \cos(2\phi) - 1]}{8\mu [3\mu_4 \cos^2(2\phi) + \mu_4 + 3\mu]}, \quad (50)$$

and the axial stretch increases if  $A_{21} > 0$  and decreases if  $A_{21} < 0$ . Solving equation (50), we obtain

$$\Phi = \Phi_m = \frac{1}{2} \arccos \frac{1}{3} \approx 35.3^\circ, \quad (51)$$

where  $\Phi_m$  represents the ‘magic angle’ [10, p. 337]. In this case, we note that, as the denominator of  $A_{21}$  is always positive and (51) is independent of the random material parameters  $\mu$  and  $\mu_4$ , there is no uncertainty to be resolved regarding this instability. For the deterministic cases where  $\mu_4 = 1$ ,  $\mu \in \{0.01, 0.02, \dots, 0.1, 0.2, \dots, 1\}$ , the values of  $A_{11}$  and  $A_{21}$  are represented graphically in Figure 6.

## 4.2 Likely chirality of the stochastic tube

Next, we assume that the angle of a preferred direction is kept fixed while the other angle can vary [11]. If the radius and axial length of the tube do not change, the condition that the torsion parameter  $\tau$  may start to decrease when the internal pressure increases is

$$A_{31} = 0. \quad (52)$$

This is equivalent to

$$\begin{aligned} & 6\mu [2 \sin(2\Phi) + \sin(4\Phi) - 2 \sin(2\Psi) - \sin(4\Psi)] \\ &= \mu_4 [3 \sin(2\Psi) + \sin(4\Psi) - 3 \sin(2\Phi) - \sin(4\Phi) + 2 \sin(2\Phi - 2\Psi) - 3 \sin(2\Phi + 4\Psi) + 3 \sin(4\Phi + 2\Psi)], \end{aligned} \quad (53)$$

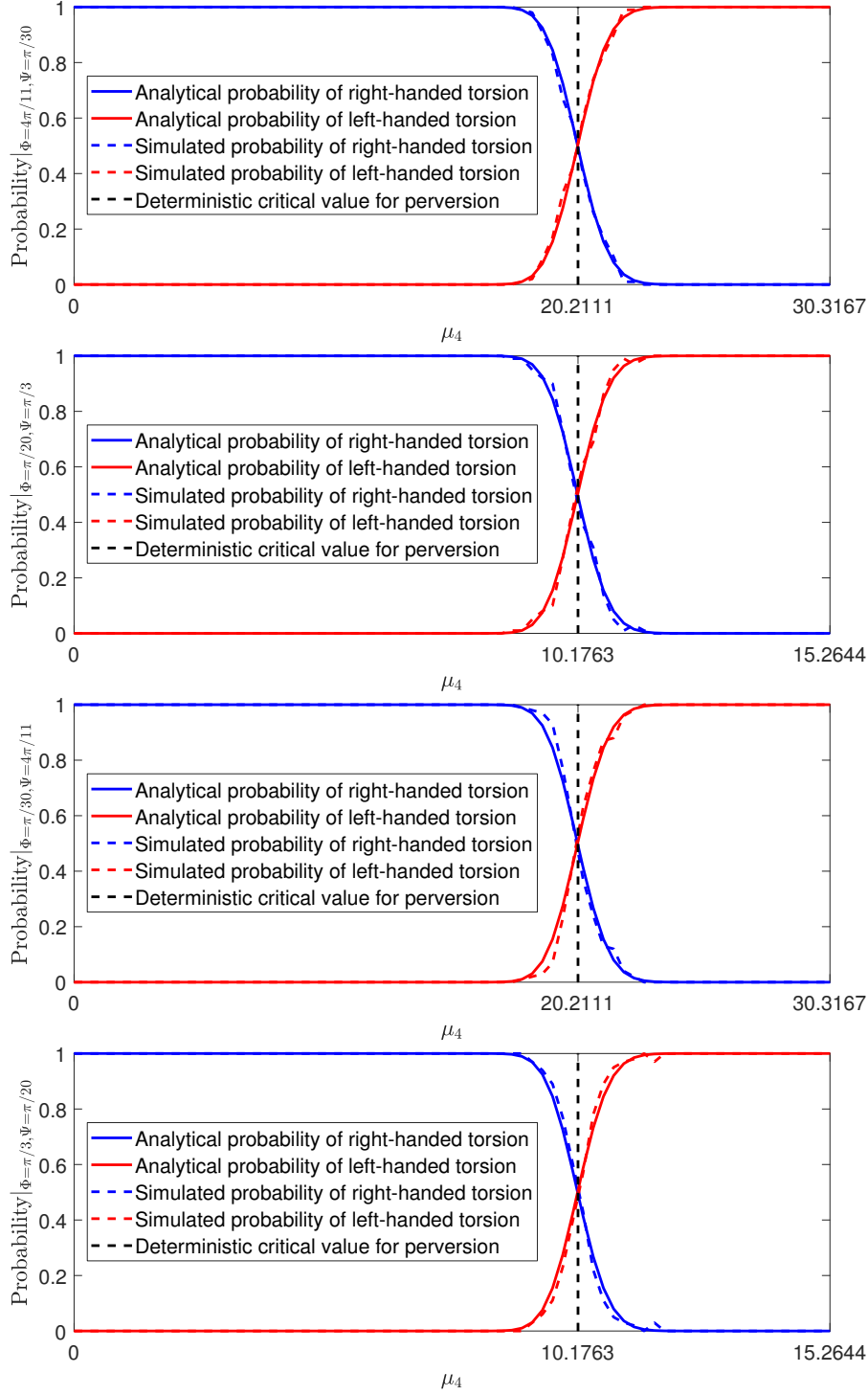


Figure 7: Probability distributions of whether perversion can occur or not for an anisotropic cylindrical tube of stochastic hyperelastic material described by (23) with the shear modulus,  $\mu$ , following a Gamma distribution with  $\rho_1 = 405$ ,  $\rho_2 = 0.01$ , and  $\mu_4$  following a Gamma distribution with  $\rho_1^{(4)} = 405$ ,  $\rho_2^{(4)} = 0.2$ , in the cases when (from top to bottom):  $\Phi = 4\pi/11$  and  $\Psi = \pi/30$ ;  $\Phi = \pi/20$  and  $\Psi = \pi/3$ ;  $\Phi = \pi/30$  and  $\Psi = 4\pi/11$ ;  $\Phi = \pi/3$  and  $\Psi = \pi/20$ . Continuous coloured lines represent analytically derived solutions, given by equations (55)-(56), while the dashed versions represent stochastically generated data composed of 100 simulations. The vertical line separates the expected regions based only on the mean value of the shear modulus,  $\underline{\mu} = \rho_1 \rho_2 = 4.05$ .

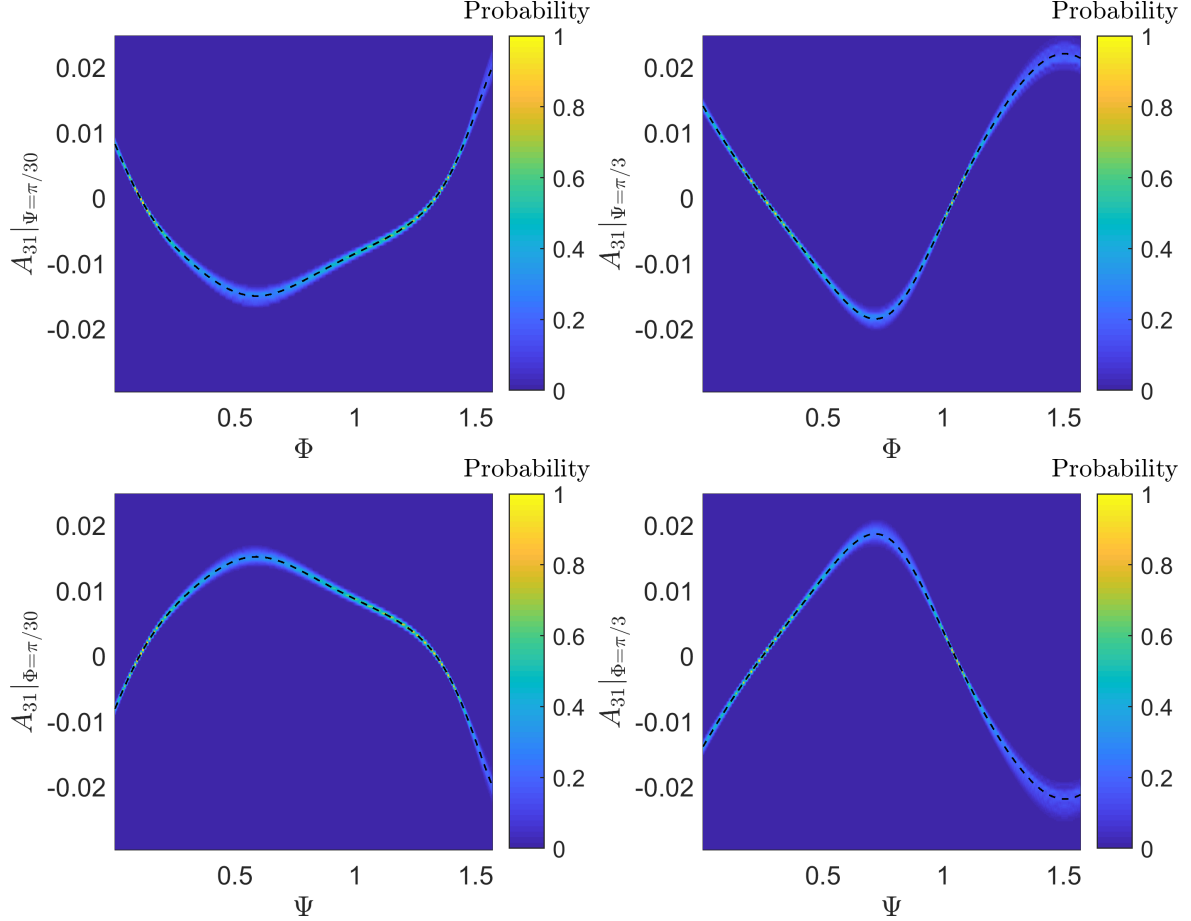


Figure 8: Probability distribution of stochastic  $A_{31}$  for the torsion of an anisotropic cylindrical tube of stochastic hyperelastic material, given by (23) with  $\mu$  drawn from a Gamma distribution with  $\rho_1 = 405$ ,  $\rho_2 = 0.01$ , and  $\mu_4$  drawn from a Gamma distribution with  $\rho_1^{(4)} = 405$ ,  $\rho_2^{(4)} = 0.2$ , in the case when:  $\Psi_0 = \pi/30$  (top-left);  $\Psi_0 = \pi/3$  (top-right);  $\Phi_0 = \pi/30$  (bottom-left);  $\Phi_0 = \pi/3$  (bottom-right). In these cases, perversion takes place with certainty at  $\Psi = \Phi_0$ , and is expected to occur also, with a given probability, for a different angle  $\Psi$ . The dashed black line corresponds to the expected value of  $A_{31}$  based only on mean parameter values,  $\underline{\mu} = \rho_1 \rho_2 = 4.05$  and  $\underline{\mu}_4 = \rho_1^{(4)} \rho_2^{(4)} = 81$ .

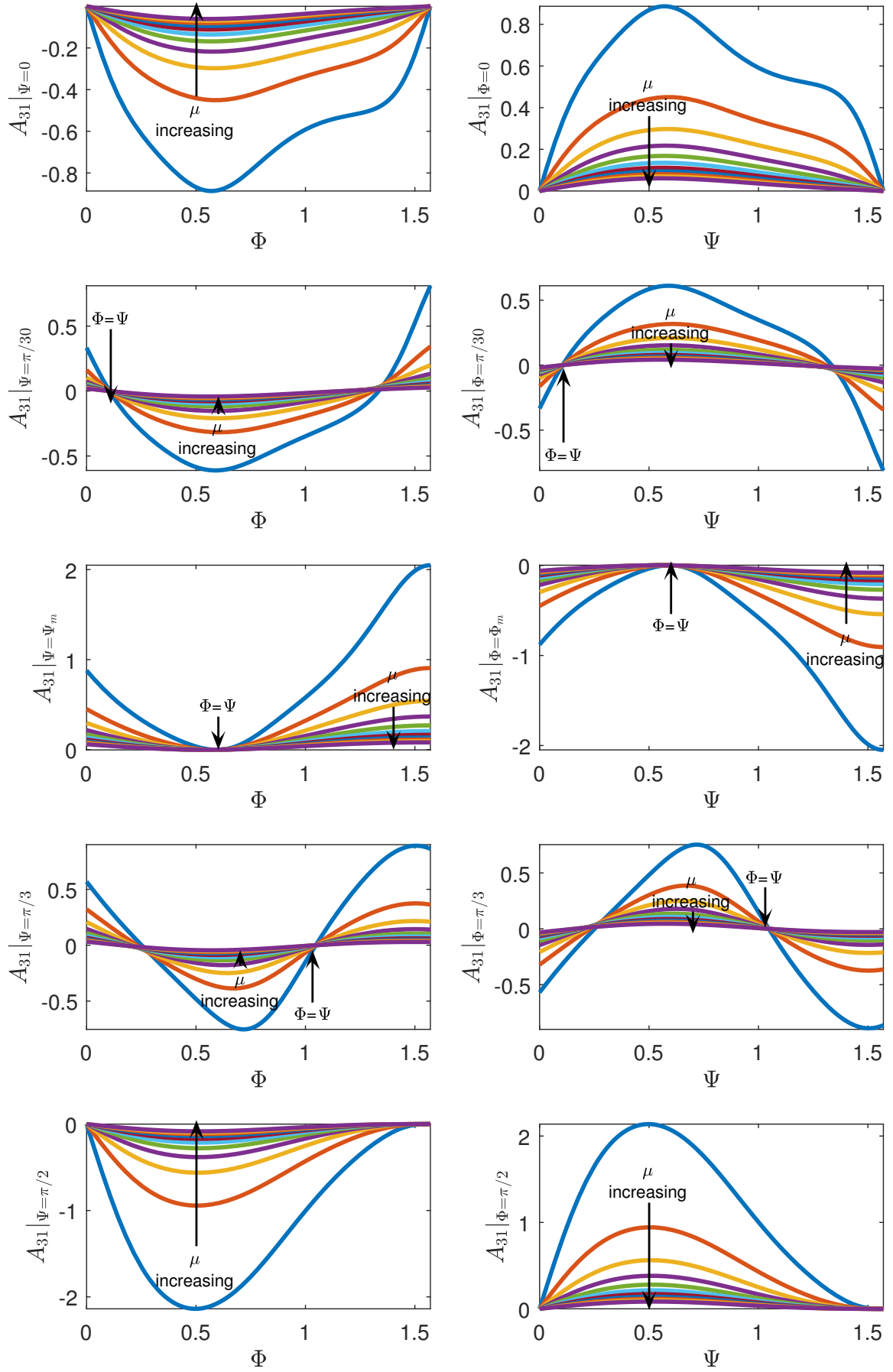


Figure 9: Deterministic values of  $A_{31}$  when  $\Psi \in \{0, \pi/30, \Psi_m, \pi/3, \pi/2\}$  is fixed and  $\Phi$  varies (left), and when  $\Phi \in \{0, \pi/30, \Phi_m, \pi/3, \pi/2\}$  is fixed and  $\Psi$  varies (right), for  $\mu_4 = 1$  and  $\mu \in \{0.1, 0.2, \dots, 1\}$  (the direction of increasing values of  $\mu$  is indicated by arrow).

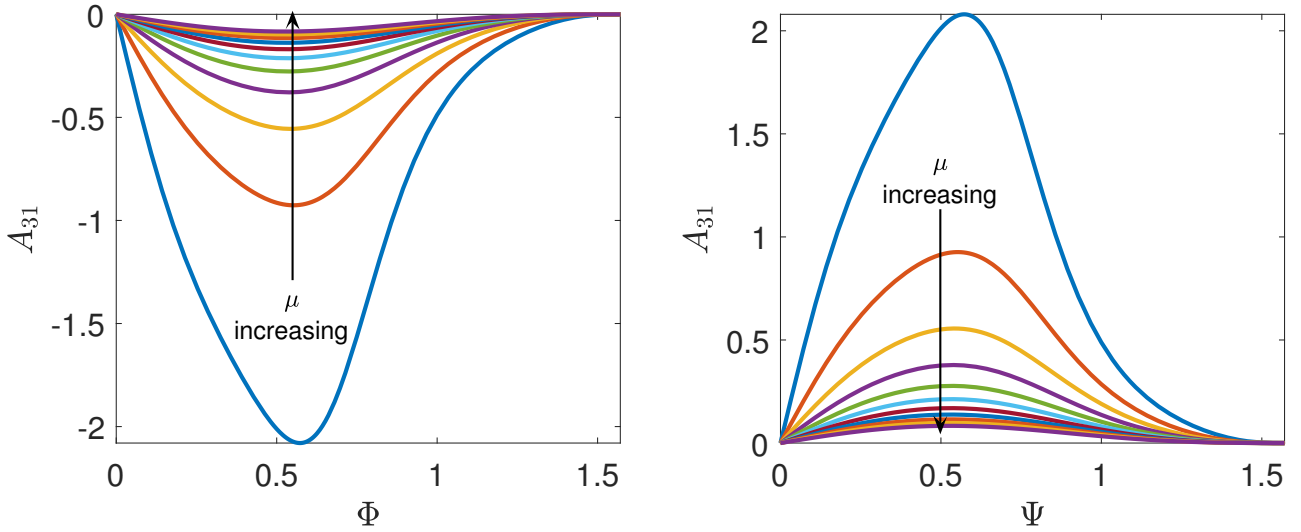


Figure 10: The values of  $A_{31}$  in the case of a single family of right-handed fibres (left), or left-handed fibres (right), for  $\mu_4 = 1$  and  $\mu \in \{0.1, 0.2, \dots, 1\}$  (the arrow shows the direction of increasing values of  $\mu$ ).

which is clearly satisfied when  $\Phi = \Psi$ , or if  $\Phi \in \{0, \pi/2\}$  and  $\Psi \in \{0, \pi/2\}$ .

When  $\Phi \neq \Psi$  and either  $\Phi \notin \{0, \pi/2\}$  or  $\Psi \notin \{0, \pi/2\}$ , we define

$$\xi = \frac{3 \sin(2\Psi) + \sin(4\Psi) - 3 \sin(2\Phi) - \sin(4\Phi) + 2 \sin(2\Phi - 2\Psi) - 3 \sin(2\Phi + 4\Psi) + 3 \sin(4\Phi + 2\Psi)}{6 [2 \sin(2\Phi) + \sin(4\Phi) - 2 \sin(2\Psi) - \sin(4\Psi)]}, \quad (54)$$

and distinguish the following cases:

(i) When  $\Psi = \Psi_0$  is fixed and  $\Phi \in (0, \pi/2) \setminus \{\Psi_0\}$ :

- (i<sub>1</sub>) if  $\Psi_0 \in \{0, \pi/2\}$ , then  $A_{31} < 0$ , i.e., there is left-handed (clockwise) twist;
- (i<sub>2</sub>) if  $\Psi_0 = \Psi_m$ , where  $\Psi_m$  is the magic angle given by (51), then  $A_{31} > 0$ , i.e., there is right-handed (anti-clockwise) twist;
- (i<sub>3</sub>) if  $0 < \Psi_0 < \Psi_m$ , then  $A_{31} > 0$  (right-handed twist) when  $\Phi < \Psi_0$ , and there exists  $\Phi^* > \Psi_0$ , such that  $A_{31} < 0$  (left-handed twist) when  $\Psi_0 < \Phi < \Phi^*$  and  $A_{31} > 0$  (right-handed twist) when  $\Phi^* < \Psi < \pi/2$ . Hence, a first inversion from right-handed to left-handed twist occurs at  $\Phi = \Psi_0$ , and a second one from left-handed to right-handed twist takes place at  $\Phi = \Phi^*$ . Then, if  $\Psi_0 < \Phi < \pi/2$ , the torsion parameter  $\tau$  increases (i.e.,  $A_{31} > 0$ ) when  $\mu > \mu_4/\xi$  and decreases when  $0 < \mu < \mu_4/\xi$ , and if  $\Phi < \Psi$ , the torsion parameter increases when  $0 < \mu < \mu_4/\xi$  and decreases (i.e.,  $A_{31} < 0$ ) when  $\mu > \mu_4/\xi$ . Thus, the probability distribution of right-handed torsion, such that  $\tau$  monotonically increases as the internal pressure increases, is

$$P_3(\mu_4) = 1 - \int_0^{\mu_4/\xi} g(u; \rho_1, \rho_2) du, \quad (55)$$

and that of left-handed torsion, such that  $\tau$  decreases as the pressure increases, is

$$P_4(\mu_4) = 1 - P_3(\mu_4). \quad (56)$$

- (i<sub>4</sub>) if  $\Psi_m < \Psi_0 < \pi/2$ , then  $A_{31} > 0$  (right-handed twist) when  $\Phi > \Psi_0$ , and there exists  $\Phi^* < \Psi_0$ , such that  $A_{31} > 0$  (right-handed twist) when  $0 < \Phi < \Phi^*$  and  $A_{31} < 0$  (left-handed twist) when  $\Phi^* < \Psi < \Psi_0$ . In this case, the first inversion from right-handed to left-handed twist occurs at  $\Phi = \Phi^*$ , and the second one from left-handed to right-handed twist at  $\Phi = \Psi_0$ .

Hence, for  $0 < \Phi < \Psi_0$ , the probability of right-handed torsion is  $P_4(\mu_4)$ , given by (56), and that of left-handed torsion is  $P_3(\mu_4)$ , given by (55).

(ii) When  $\Phi = \Phi_0$  is fixed and  $\Psi \in (0, \pi/2) \setminus \{\Phi_0\}$ :

(ii<sub>1</sub>) if  $\Phi_0 \in \{0, \pi/2\}$ , then  $A_{31} > 0$ , i.e., there is right-handed twist;

(ii<sub>2</sub>) if  $\Phi_0 = \Phi_m$ , where  $\Phi_m$  is the magic angle given by (51), then  $A_{31} < 0$ , i.e., there is left-handed twist;

(ii<sub>3</sub>) if  $0 < \Phi_0 < \Phi_m$ , then  $A_{31} < 0$  (left-handed twist) when  $0 < \Psi < \Phi_0$ , and there exists  $\Psi^* > \Phi_0$ , such that  $A_{31} > 0$  (right-handed twist) when  $\Phi_0 < \Psi < \Psi^*$  and  $A_{31} < 0$  (left-handed twist) when  $\Psi^* < \Psi < \pi/2$ . Hence, a first inversion from left-handed to right-handed twist takes place at  $\Psi = \Phi_0$ , and a second one from right-handed to left-handed twist at  $\Psi = \Psi^*$ .

Then, for  $\Psi_0 < \Phi < \pi/2$ , the probability of right-handed torsion is  $P_4(\mu_4)$ , given by (56), and that of left-handed torsion is  $P_3(\mu_4)$ , given by (55).

(ii<sub>4</sub>) if  $\Phi_m < \Phi_0 < \pi/2$ , then  $A_{31} < 0$  (left-handed twist) when  $\Phi_0 < \Psi < \pi/2$ , and there exists  $\Psi^* < \Phi_0$ , such that  $A_{31} < 0$  (left-handed twist) when  $0 < \Psi < \Psi^*$  and  $A_{31} > 0$  (right-handed twist) when  $\Psi^* < \Psi < \Phi_0$ . In this case, the first inversion from left-handed to right-handed twist occurs at  $\Psi = \Psi^*$ , and the second one from left-handed to right-handed twist at  $\Psi = \Phi_0$ .

Hence, for  $0 < \Phi < \Psi_0$ , the probability of right-handed torsion is  $P_3(\mu_4)$ , given by (55), and that of left-handed torsion is  $P_4(\mu_4)$ , given by (56).

When  $\rho_1 = 405$  and  $\rho_2 = 0.01$  (see Figure 3 - left), the probability distributions given by equations (55)-(56) are illustrated numerically in Figure 7, where the different plots, from top to bottom, correspond, respectively, to the cases: (i<sub>3</sub>) with  $\Phi = 4\pi/11$  and  $\Psi = \pi/30$ ; (i<sub>4</sub>) with  $\Phi = \pi/20$  and  $\Psi = \pi/3$ ; (ii<sub>3</sub>) with  $\Phi = \pi/30$  and  $\Psi = 4\pi/11$ ; (ii<sub>4</sub>) with  $\Phi = \pi/3$  and  $\Psi = \pi/20$  (blue lines for  $P_3$  and red lines for  $P_4$ ). In each case,  $\mu_4 \in (0, 2\xi\mu)$  was divided into 100 steps, then for each value of  $\mu_4$ , 100 random values of  $\mu$  were numerically generated from the specified Gamma distribution and compared with the inequalities defining the two intervals for values of  $\mu_4$ . For example, if  $\mu_4$  follows a Gamma distribution with  $\rho_1^{(4)} = 405$ ,  $\rho_2^{(4)} = 0.2$  (see Figure 3 - right), then perversion will take place with certainty at  $\Phi = \Psi$ , and is expected to occur also, with a given probability, at a different angle, as seen from Figure 8.

For the deterministic cases where  $\mu_4 = 1$ ,  $\mu \in \{0.1, 0.2, \dots, 1\}$ , the values of  $A_{31}$  are illustrated graphically in Figure 9, where  $\Psi_0 \in \{0, \pi/30, \Psi_m, \pi/3, \pi/2\}$  (left) and  $\Phi_0 \in \{0, \pi/30, \Phi_m, \pi/3, \pi/2\}$  (right). From these plots, we see that a pressurised tube with a right-handed family of fibres deforms by a left-handed torsion if the other fibres are kept either horizontal or vertical (top and bottom left), and a tube with a left-handed family of fibres deforms by a right-handed torsion if the other fibres are horizontal or vertical (top and bottom right). This is the expected behaviour in the case of a single family of fibres as well [11] (see Figure 10).

## 5 Conclusion

We have examined the elastic response of a stochastic fibre-reinforced tube under three typical combined loadings. In the deterministic case, there is a strict transition between different behaviours, given by a single numerical value. As expected, in the stochastic case, our analysis identifies probabilistic intervals where the two different states compete and both have a quantifiable chance to be presented. Outside these intervals, the system behaves very closely to a deterministic one. In the present computations, the probabilistic intervals are relatively small, indicating that the phenomena of perversion and inversion in these systems are strongly driven by the geometry of the fibres. Here, we have not included stochastic variations in the fibre angles. This type of study has been carried out extensively by various authors [8, 24] who homogenised the effects of stochastic dispersion so that it enters as a parameter in the deterministic setting. Nevertheless, our approach can be extended directly to the problem of fibre dispersion to reveal the full effect of stochasticity. This type of analysis has important applications, such as soft biological tissues (e.g., plants, arterial walls) and engineered

structures (e.g., soft actuators) at large strains, where mathematical models that take into account the variability in the material responses are crucial.

**Acknowledgement.** The support for Alain Goriely by the Engineering and Physical Sciences Research Council of Great Britain under research grant EP/R020205/1 is gratefully acknowledged.

## References

- [1] Abramowitz M, Stegun IA. 1964. Handbook of Mathematical Functions with Formulas, Graphs, and Mathematical Tables, National Bureau of Standards, Applied Mathematics Series, vol. 55, Washington.
- [2] Aguiar AR, Lopes da Rocha G. 2018. On the number of invariants in the strain energy density of an anisotropic nonlinear elastic material with two material symmetry directions, *Journal of Elasticity* 131, 125-132.
- [3] Aguiar AR, Lopes da Rocha G. 2018. Erratum to: On the number of invariants in the strain energy density of an anisotropic nonlinear elastic material with two material symmetry directions, *Journal of Elasticity* 131, 133-136.
- [4] Bertinetti L, Fischer FD, Fratzl P. 2013. Physicochemical basis for water-actuated movement and stress generation in nonliving plant tissues, *Physical Review Letters* 111, 238001.
- [5] Connolly F, Polygerinos P, Walsh CJ, Bertoldi K. 2015. Mechanical programming of soft actuators by varying fiber angle, *Soft Robotics* 2, 26-32.
- [6] Connolly F, Walsh CJ, Bertoldi K. 2017. Automatic design of fiber-reinforced soft actuators for trajectory matching, *Proceedings of the National Academy of Sciences of the United States of America (PNAS)* 114, 51-56.
- [7] Caylak I, Penner E, Dridger A, Mahnken R. 2018. Stochastic hyperelastic modeling considering dependency of material parameters, *Computational Mechanics* (doi: 10.1007/s00466-018-1563-z).
- [8] Gasser TC, Ogden RW, Holzapfel GA. 2006. Hyperelastic modelling of arterial layers with distributed collagen fibre orientations, *Journal of the Royal Society Interface* 3, 15-35.
- [9] Gilchrist MD, Murphy JG, Pierrat B, Saccomandi G. 2017. Slight asymmetry in the winding angles of reinforcing collagen can cause large shear stresses in arteries and even induce buckling, *Meccanica* 52, 3417-3429.
- [10] Goriely A. 2017. *The Mathematics and Mechanics of Biological Growth*, Springer-Verlag, New York.
- [11] Goriely A, Tabor M. 2013. Rotation, inversion and perversion in anisotropic elastic cylindrical tubes and membranes, *Proceedings of the Royal Society A* 469, 2013001.
- [12] Goriely A, Tabor M. 1998. Spontaneous helix-hand reversal and tendril perversion in climbing plants, *Physical Review Letters* 80, 1564-1567.
- [13] Grimmett GR, Stirzaker DR. 2001. *Probability and Random Processes*, 3rd ed, Oxford University Press, Oxford.
- [14] He, L, Lou J, Du J. 2018. Voltage-driven torsion of electroactive thick tubes reinforced with helical fibers, *Acta Mechanica* 229, 2117-2131.
- [15] Hughes I, Hase TPA. 2010. *Measurements and Their Uncertainties: A Practical Guide to Modern Error Analysis*, Oxford University Press, Oxford.
- [16] Jaynes ET. 1957. Information theory and statistical mechanics i, *Physical Review* 108, 171-190.



- [17] Jaynes ET. 1957. Information theory and statistical mechanics ii, *Physical Review* 106, 620-630.
- [18] Jaynes ET. 2003. *Probability Theory: The Logic of Science*, Cambridge University Press, Cambridge, UK.
- [19] Johnson NL, Kotz S, Balakrishnan N. 1994. *Continuous Univariate Distributions*, Vol 1, 2nd edition, John Wiley & Sons, New York.
- [20] Kroeger M, Karl H, Simmler B, Singer P. 2018. Viability Test Device for anisakid nematodes, *Heliyon*, 2018 4, e00552.
- [21] Mathai AM. 1982. Storage capacity of a dam with Gamma type inputs, *Annals of the Institute of Statistical Mathematics* 34, 591-597.
- [22] McCoy JJ. 1973. A statistical theory for predicting response of materials that possess a disordered structure, Technical report ARPA 2181, AMCMS Code 5911.21.66022, Army Materials and Mechanics Research Center, Watertown, Massachusetts.
- [23] McMillen T, Goriely A, 2002. Tendril perversion in intrinsically curved rods, *Journal of Nonlinear Science* 12, 241-281.
- [24] Melnik AV, Da Rocha HB, Goriely A. 2015. On the modeling of fiber dispersion in fiber-reinforced elastic materials *International Journal of Non-Linear Mechanics* 75, 92-106.
- [25] Mihai LA, Goriely A. 2011. Positive or negative Poynting effect? The role of adscititious inequalities in hyperelastic materials, *Proceedings of the Royal Society A* 467, 3633-3646.
- [26] Mihai LA, Goriely A. 2013. Numerical simulation of shear and the Poynting effects by the finite element method: An application of the generalised empirical inequalities in non-linear elasticity, *International Journal of Non-Linear Mechanics* 49, 1-14.
- [27] Mihai LA, Goriely A. 2017. How to characterize a nonlinear elastic material? A review on nonlinear constitutive parameters in isotropic finite elasticity, *Proceedings of the Royal Society A* 473, 20170607 (doi: 10.1098/rspa.2017.0607).
- [28] Mihai LA, Woolley TE, Goriely A. 2018. Stochastic isotropic hyperelastic materials: constitutive calibration and model selection, *Proceedings of the Royal Society A* 474, 20170858.
- [29] Mihai LA, Woolley TE, Goriely A. 2018. Likely equilibria of the stochastic Rivlin cube, *Philosophical Transactions of the Royal Society A*, 20180068 (doi: 10.1098/rsta.2018.0068).
- [30] Mihai LA, Fitt D, Woolley TE, Goriely A. 2018. Likely cavitation in stochastic elasticity, *Journal of Elasticity*, (doi: 10.1007/s10659-018-9706-1).
- [31] Mihai LA, Fitt D, Woolley TE, Goriely A. 2018. Likely equilibria of stochastic hyperelastic spherical shells and tubes, *Mathematics and Mechanics of Solids*, to appear (arXiv:1808.02110).
- [32] Moschopoulos PG. 1985. The distribution of the sum of independent Gamma random variables 37, 541-5544.
- [33] Nörenberg N, Mahnken R. 2015. Parameter identification for rubber materials with artificial spatially distributed data, *Computational Mechanics* 56, 353370.
- [34] Oden JT. 2018. Adaptive multiscale predictive modelling, *Acta Numerica* 27, 353-450.
- [35] Ogden RW. 1997. *Non-Linear Elastic Deformations*, 2nd ed, Dover, New York.
- [36] Ostoja-Starzewski M. 2007. *Microstructural Randomness and Scaling in Mechanics of Materials*, CRC Press.

- [37] Quarteroni A, Lassila T, Rossi S, Ruiz-Baier R. 2017. Integrated heart - Coupling multiscale and multiphysics models for the simulation of the cardiac function, *Computer Methods in Applied Mechanics and Engineering* 314, 345-407.
- [38] Shannon CE. 1948. A mathematical theory of communication, *Bell System Technical Journal* 27, 379-423, 623-659.
- [39] Soni J, Goodman R. 2017. *A Mind at Play: How Claude Shannon Invented the Information Age*, Simon & Schuster, New York.
- [40] Soize C. 2000. A nonparametric model of random uncertainties for reduced matrix models in structural dynamics, *Probabilistic Engineering Mechanics* 15, 277-294.
- [41] Soize C. 2001. Maximum entropy approach for modeling random uncertainties in transient elastodynamics, *Journal of the Acoustical Society of America* 109, 1979-1996.
- [42] Spencer AJM. 1971. Theory of invariants. In: Eringen, A.C. (ed.) *Continuum Physics* 1, 239-253, Academic Press, New York.
- [43] Staber B, Guilleminot J. 2015. Stochastic modeling of a class of stored energy functions for incompressible hyperelastic materials with uncertainties, *Comptes Rendus Mécanique* 343, 503-514.
- [44] Staber B, Guilleminot J. 2016. Stochastic modeling of the Ogden class of stored energy functions for hyperelastic materials: the compressible case, *Journal of Applied Mathematics and Mechanics/Zeitschrift für Angewandte Mathematik und Mechanik* 97, 273-295.
- [45] Staber B, Guilleminot J. 2017. Stochastic hyperelastic constitutive laws and identification procedure for soft biological tissues with intrinsic variability, *Journal of the Mechanical Behavior of Biomedical Materials* 65, 743-752.
- [46] Staber B, Guilleminot J. 2018. A random field model for anisotropic strain energy functions and its application for uncertainty quantification in vascular mechanics, *Computer Methods in Applied Mechanics and Engineering* 333, 94-113.
- [47] Sullivan TJ. 2015. *Introduction to Uncertainty Quantification*, Springer-Verlag, New York.
- [48] Truesdell C, Noll W. 2004. *The Non-Linear Field Theories of Mechanics*, 3rd ed, Springer-Verlag, New York.